





Optics Letters

Efficient fabrication of a high-aspect-ratio AFM tip by one-step exposure of a long focal depth holographic femtosecond axilens beam

DENG PAN,¹ SHUNLI LIU,¹ SHENGYUN JI,¹ ZE CAI,¹ JIAWEN LI,^{1,2}  YAOPING HOU,¹ WEIJIE ZHANG,¹ SHENGYING FAN,¹ RUI LI,¹ YANLEI HU,¹  WULIN ZHU,¹ DONG WU,^{1,2,3} AND JIARU CHU¹

¹CAS Key Laboratory of Mechanical Behavior and Design of Materials, Department of Precision Machinery and Precision Instrumentation, University of Science and Technology of China, Hefei, Anhui 230027, China

²e-mail: jwl@ustc.edu.cn

³e-mail: dongwu@ustc.edu.cn

Received 26 November 2019; revised 11 January 2020; accepted 13 January 2020; posted 13 January 2020 (Doc. ID 384249); published 10 February 2020

In this Letter, we demonstrate a laser fabrication strategy that uses the long focal depth femtosecond axilens laser beam to manufacture the high-aspect-ratio (HAR) micropillars and atomic force microscopy (AFM) probes by one-step exposure. The long depth of focus is generated by modulating laser beam focused at different positions. By adjusting the exposure height, the morphology of HAR micropillars can be tuned flexibly, and the micropillar with an ultra-high aspect ratio (diameter of 1.5 μm , height of 102 μm , AR = 70) can be fabricated within 10 ms which is a great challenge for other processing methods to obtain such a HAR microstructure in such a short time. In addition, the HAR micropillar is fabricated onto a cantilever to form the AFM probe. The homemade probe shows fine imaging quality. This method greatly improves the processing efficiency while ensuring the fabrication resolution which provides a powerful method for processing HAR microstructures. © 2020 Optical Society of America

<https://doi.org/10.1364/OL.384249>

The improvement of surface science is greatly promoted by the scanning-probe microscopy (SPM), and the performance of SPM depends largely on the morphology and composition of the probe [1]. Atomic force microscopy (AFM) is one of the most successful scanning-probe microscopies which consists of a cantilever beam and a high-aspect-ratio (HAR) tip [2]. The commercial HAR tips are usually silicon-based materials prepared by the complex etching process. Due to the limitation of the materials etching, the tip geometries are typically confined to cones or pyramids with a limited aspect ratio [3]. However, with AFM technology being applied in more applications, the need to develop a tailed AFM tip is critical. Correspondingly, a variety of manufacturing techniques have been developed, for example, silicon etching, compressible replica molding, and two-photo polymerization (2PP) [4–6].

Among these manufacturing methods, 2PP is a promising means with the advantages of excellent flexibility, true three-dimensional processing ability, and high resolution and fabricating ultra-high-aspect-ratio microstructures [7,8]. There have been some reports on the use of 2PP processing probes. For example, Göring *et al.* fabricated the tailored probes by 2PP and tuned the resonance spectrum by adding the rebar structures [9]. Alsharif *et al.* printed not only the probe, but also the cantilever; the AFM probe shows a larger bandwidth in contact mode [10]. In these works, the tailored AFM probes with a sharp tip and arbitrary shape which were manufactured by 2PP demonstrate the good imaging quality, customizable capabilities, and durability, which proves that this method for fabricating AFM probes has promising prospects.

However, the low processing efficiency of 2PP has become a bottleneck restricting its further application because of the time-consuming point-by-point scanning strategy [11]. For example, the resolution of a common 2PP system is 800 nm \times 800 nm \times 1.5 μm which means that it takes several hours to fabricate a tailored AFM probes and even several days to fabricate a HAR AFM probe array. An alternative to solve this problem is to introduce the spatial light modulator (SLM) which can modulate the phase of the femtosecond laser beam into a 2PP processing system. In theory, arbitrary-shaped beams can be generated by modulating the beam wavefront. Therefore, the point-by-point processing upgrades to layer-by-layer, even voxel-by-voxel processing, leading to great improvement of processing efficiency.

The axilens beam combines the properties of the long focal depth of the axicon beam and the high energy concentration of conventional spherical beams and can be used to achieve a long focal depth without significant sacrifice in numerical aperture [12]. Since its demonstration in 1991, the axilens beam has been used in a variety of applications such as particle manipulation, holographic projection, imaging, and micro-hole drilling [13–15]. So far, to the best of our knowledge, there are no

reports about the use of a femtosecond axilens beam to process HAR microstructures.

Here, we introduce the SLM into the conventional 2PP system and fabricated HAR micropillars and AFM probes only by one-step exposure. By loading the axilens hologram onto the SLM, the long depth of focus (LDOF) is generated and used to fabricate HAR micropillars by single exposure. By modulating the phase on the diffractive plane, the laser beam can focus at different positions and form the LDOF. Due to the propagation characteristics of the axilens beam, side-lobe structures (SLSs) will be exposed inevitably. Therefore, we use the method of controlling the depth of processing to avoid the appearance of SLS and obtain the ultra-high-aspect-ratio micropillars. The tips of these micropillars have a small radius, and thus we used four AFM probes to obtain excellent imaging results. This time-saving method greatly improves the processing efficiency (> 100 times) while ensuring the fabrication resolution which is suitable for the mass production. Besides, to the best of our knowledge, this is the first time the axilens beam has been used to fabricate HAR micropillars and microstructures by TPP single exposure.

In order to generate the axilens beam, we modify the spherical phase and extend the focus along the propagation direction. The spherical phase with a wavelength λ can be written as $\varphi = \left(\frac{2\pi}{\lambda}\right) * \sqrt{r^2 + f^2}$, where r is the distance from the diffraction plane to the focus point, and f is the predesigned focal length. Using binomial expansion to simplify the formula, the spherical phase can be written as $\varphi = \left(\frac{2\pi r^2}{2\lambda f}\right) = \frac{\pi r^2}{\lambda f}$. When we need to lengthen the focus, f becomes a function of the distance r ; thus, φ can be written as $\varphi = \frac{\pi r^2}{\lambda f(r)}$. The $f(r)$ can be considered as a polynomial form $f(r) = f_0 + m * r^n$, and f_0 is the distance from focus to the position where the beam starts focusing. Thus, we need to determine the values of m and n . For the LDOF, it is hoped that the focus can have uniform energy distribution within the focus range. Therefore, m and n should satisfy $\Delta f(r) = 2mr \Delta(r)$. Thus, $n = 2$, and $m = \Delta z / R^2$, where the R is the radius of the diffraction plane. In summary, the phase of the LDOF can be written as $\varphi = \frac{\pi r^2}{\lambda(f_0 + \frac{\Delta z}{R^2} r^2)}$, and the calculated hologram is shown in Fig. 1(a). By modulating the spherical phase, the laser beam is focused at different positions, and the axilens beam with a LDOF is generated. Actually, the Bessel beam focused by an axicon also has a LDOF.

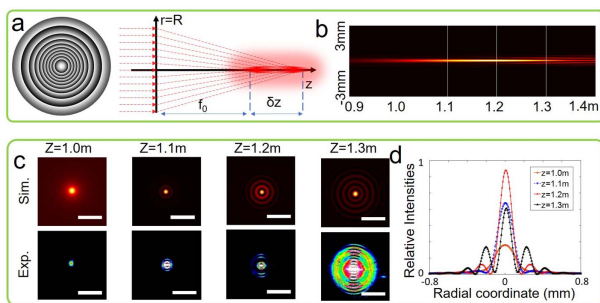


Fig. 1. Generation of axilens beam with a long focal depth. (a) Hologram used to generate a long focal depth and the principle of generating long focus. (b) Simulation results of DOF calculated by Fresnel diffraction. (c) Simulation and experimental results of different propagation distances (0.15, 0.35, 0.55, and 0.75 m). (d) Relative intensities of propagation distances at 0.15, 0.55, and 0.95 m.

However, the focus distance f_0 and the focus length Δz are only regulated by an axicon radius, axicon top corner, and laser beam diameter, because the axicon has a triangular cross shape, which is inflexible and inconvenient to be adjusted in processing and imaging systems that are already fixed in size. Here, the Fresnel diffraction theory is used to obtain the diffraction of the LDOF in free space [Fig. 2(b)]. With the increase of propagation distance, the beam gradually focuses, and the beam energy begins to concentrate at a predesigned position. However, due to the inherent characteristics of light propagation along a straight line, as the diffraction distance increases further, the SLS inevitably appears gradually around the main-lobe. Figure 2(c) shows the simulation and experimental diffraction results at different propagation distances ($z = 1.0, 1.1, 1.2$, and 1.3 m) in the x - y plane. Because the sub-lobes are redundant for the laser processing, it is necessary to figure out the relationship of energy distribution between the sub-lobes and the main-lobe. Figure 2(d) describes the calculated light intensity distribution results at different diffraction distances. When $Z = 1.0$ m, the beam just starts to focus, so the focus energy is relatively low. As $z = 1.1/1.2$ m, the center energy continually increases and the energy of the sub-lobe is about one-tenth of the main-lobe. When $Z = 1.3$ m, the beam is about to stop focusing, and the energy of the main-lobe decreases, while the energy of the sub-lobe increases. However, the sub-lobe energy is still only 40% of the main-lobe. Because the 2PP is a nonlinear process, and the energy of the side-lobes does not exceed one-half of the main-lobe, the influence caused by the sub-lobe can be eliminated through regulating the energy.

In order to fabricate HAR micropillars by one-step axilens beam exposure, the LDOF needs to be reconstruct under the objective lens. Here, a 4f system consisting of an objective lens and a normal lens is used to shrink and reconstruct the axilens beam for further 2PP fabrication [Fig. 2(a)]. It is worth mentioning that the Bessel beam is used in 2PP for the rapid fabrication of a microring structure and microtubes with very high quality. However, the Bessel beam is focused by a 4f system and an objective, which leads to a short focal depth (about $10 \mu\text{m}$) and is not suitable for the fabrication of HAR micropillars. Here, the expanded femtosecond laser (central

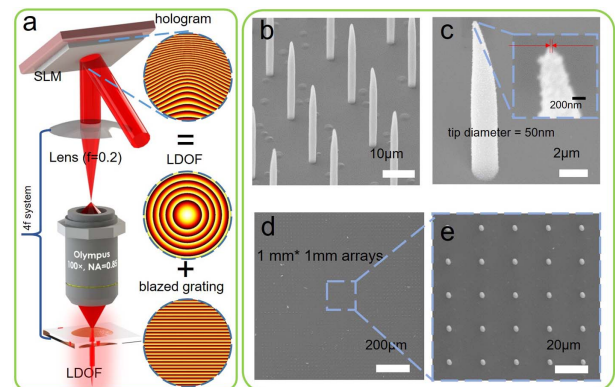


Fig. 2. Schematic of a single exposure processing high-aspect-ratio micropillar 2PP system. (a) Fabrication system mainly composed of the SLM, lens, and objective lens. (b) Side view of the micropillar fabricated by the single exposure. (c) Micropillar with tip diameter is 50 nm. (d) and (e) Large-area micropillar array (1 mm \times 1 mm) fabricated by single exposure; the whole processing time is about 10 min. The laser power used in all fabrications is 100 mW.

wavelength $\lambda = 800$ nm, pulse repetition rate $f = 80$ MHz, and pulse width $\tau = 75$ fs) are projected onto the SLM. The phase displayed on the SLM is composed of two parts: the LDOF part and blazed grating part. The function of the blazed grating is to separate the LDOF from the zero order light. After being modulated by the SLM, the laser beam is focused by a lens ($f = 0.2$ m) and an objective lens ($100\times$, air, NA = 0.85). As a result, the elongated laser focus is focused into the underlying photoresist (SZ2080). Therefore, the HAR micropillars can be fabricated by one-step exposure. Finally, the sample is developed in 1 propanol and dried with a CO₂ critical point dryer to avoid the capillary force to complete the preparation of the HAR micropillars [Fig. 2(b)]. Different from conventional 2PP based on point-by-point scanning which requires a lot of time, this single exposure method can manufacture a HAR micropillar within a short time. Depending on the different laser powers, the processing time by this method is about 5–200 ms, which is one-tenth to one-hundredth of the point-by-point processing times. It is worthy noting that after CO₂ critical point drying, the diameter of the micropillar tip is about 50 nm, which is far beyond the optical diffraction limit [Fig. 2(c)]. The possible reason for this phenomenon is the nonlinearity of energy absorption during the 2PP process, which causes the small feature size. Using this LDOF phase-assisted processing method, an ultra-fast process for fabricating large-area microstructures can be achieved. We fabricated a 1 mm \times 1 mm array with a period of 20 μ m for each micropillar [Figs. 2(d) and 2(e)]. The height of the micropillar is about 30 μ m, and the total number of micropillars is 2500. The processing time for each micropillar is 100 ms, and the total time is about 10 min. In fact, the fabrication of micropillars takes only 4 min, and the other time is consumed in manual stitching and alignment between arrays. In comparison, the processing time is about 110 min by a conventional point-to-point 2PP, which will linearly increase as the height of the micropillars rises.

As mentioned above, the sub-lobe of the LDOF appears as the propagation distance increases. Hence, in order to fabricate HAR microstructures, these side-lobes should be avoided. Besides, owing to the fact that the photoresist faces up, the exposure depth has great impact on the morphology and the height. Figures 3(a)–3(d) illustrate four kinds of micropillar morphologies fabricated with the LDOF hologram ($f_0 = 1.2$ m, $\Delta z = 1$ m). As the exposure depth increases from 5 to 20 μ m, the obtained microstructures are gradually higher, and the first-order, second-order, and third-order SLSs gradually appear. In order to distinguish each lobe clearly, SEM photos in Figs. 3(a)–3(d) are colored and the main-lobe, first-order, second-order, and third-order sub-lobe are expressed in yellow, red, green, and blue, respectively.

Since our goal is the rapid processing of HAR micropillars, it is necessary to increase the micropillar length while avoiding the presence of other interfering structures. Two strategies are adopted. (1) As the sub-lobe only appears at the back part of the LDOF, we can keep the sub-lobe away by controlling the sample exposure position. (2) In order to get a LDOF, we can regulate the parameters of holograms displayed on the SLM. When the depth of focus in free space becomes longer, the main-lobe under the objective lens also gets extended. Figures 3(e)–3(g) show the statistical histograms of the micropillar height as the exposure distance increases (the Z-direction coordinates increase). The hologram parameters used in Figs. 3(e)–3(g)

are $f_0 = 1.2$ m, $\Delta z = 1$ m, $f_0 = 1.2$ m, $\Delta z = 1$ m, and $f_0 = 1.2$ m, $\Delta z = 1$ m, respectively, and the exposure time is 300 ms. H represents the total height of the microstructures, which increases linearly as the z increases. The h_1 , h_2 , and h_3 represent the height of the main-lobe, first-order sub-lobe, and second-order sub-lobe, respectively [illustration in Fig. 3(c)]. From the statistical results, the height gradually increases, and the sub-lobe appears in order with the increase of z , which is consistent with the distribution of the LDOF light field. However, as the f_0 decreases from 1.2 to 0.6 m, the main-lobe height increases from 35 to 120 μ m [Fig. 3(h)], because the focus position is varied forward when the f_0 decreases. This results in an increase of distance from the laser focus to the lens, which means the effective distance of the focus increases. A longer effective distance brings the ability to process higher main-lobe microstructures.

Interestingly, with the exposure depth increasing, the evolution of the micropillar's morphology is similar to the growth process of bamboo in nature, which is depicted in Figs. 3(i) and 3(j). This means that we can fabricate “bamboo-like” and “bamboo shoot-like” by controlling the exposure depth at the same time. The fabrication parameter is $f_0 = 0.5$ m, $\Delta z = 1$ m, and the exposure time is 300 ms. The micropillars fabricated by single exposure have a height of 102 μ m and a diameter of 1.5 μ m. The aspect ratio of micropillars can reach as high as 70, which is a great challenge for other processing methods to obtain such a HAR microstructure in one-step exposure. Furthermore, the “bamboo shoot-like” microstructures can be obtained by controlling the thickness and the z-direction position of the photoresist. As illustrated in Fig. 3(k), the thickness of photoresist is about 100 μ m, controlled by spin coating. The sample position was adjusted precisely so that only the sub-lobe can be focused into the photoresist, while the main-lobe is focused in the air. In this way, the bamboo-shoot-like

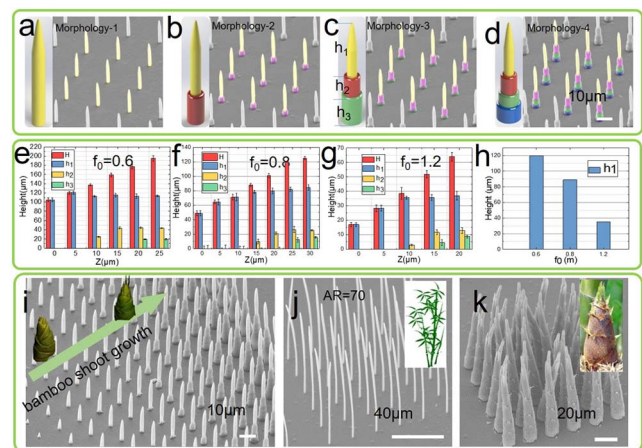


Fig. 3. Regulation of the single exposure micropillar morphology. (a)–(d) Four morphologies of the single exposure micropillar. (e)–(g) Statistics on the height of the micropillar obtained when fabricating with $f = 0.6, 0.8,$ and $1.2, z = 1$ hologram. (h) Primary height changes as the focus distance changes. (i) Side view of the micropillar array with the gradual increase of the processing depth. (j) High-aspect-ratio (> 50) micropillar fabricated by single exposure. (k) Multi-layer composite microstructure is manufactured by the single exposure, and the shape is similar to the bamboo shoot. The laser power used in (a)–(d) and (i) is 150 mW, and the laser power used in (j) and (k) is 200 mW.

microstructures with multi-annular-layered microstructures/nanostructures on the surface are obtained. This tapered multi-layered microstructure can play an important role in the field of cell analysis and cell growth research. In particular, the microstructures/nanostructures on the surface can provide the necessary adhesion sites for the cell growth, which can be used to study the cell growth, migration, and differentiation on the 3D topography.

Since the morphology of the micropillars can be adjusted flexibly, we can fabricate HAR micropillars with a sharp tip on the cantilevers to form the AFM probe (LDOF probe). As shown in Fig. 4(a), the SZ2080 was dropped onto the cantilever and heated by a hot plate at 60°C for 1 h. The LDOF is focused into the photoresist, and the LDOF probe can be fabricated by one-step exposure. The LDOF probe in Fig. 4(b) has a diameter of 1.5 μm , height of 25 μm , and AR of 16; such a cylindrical cross section with a high-aspect-ratio probe is difficult to process by other conventional methods such as etching. The AFM testing system is shown in Fig. 4(c); when the tip reaches the sample surface, the laser beam deflection caused by the cantilever is measured to calculate the surface topography of the sample. We selected a standard blend composed of polystyrene (PS) and low-density polystyrene (LDPS) (Bruker Nano Inc.) for imaging. The nominal elastic moduli of PS and LDPE are 2 GPa and 100 Mpa, respectively. The free resonance frequencies and spring constant were measured to be 403 kHz and 40 N/m, respectively. Figure 4(d) is the measured topography distribution and phase distribution results by the LDOF probe, respectively. We also use a commercial probe to measure the same samples, as shown in Fig. 4(f). From the measurement curve shown in Figs. 4(e) and 4(g), both probes can well reflect the spherical topography of the micro-PS sphere. Besides, the phase distribution can be used to distinguish the physical properties between different materials. From the results, we can clearly see that the PS spheres and substrates are well distinguished in both LDOF probes and commercial probes.

According to our test, the LDOF probes demonstrated comparable imaging traits as commercial probes. Notably, the Young's modulus of tips made of polymer is only 2.34 GPa,

which is much lower than silicon-based probes and can be regulated by changing the material and laser power. Besides, the TPP can be used to fabricate multi-material probes such as hydrogel. The fabrication time for an AFM probe in the method of 2PP assisted with the LDOF is only 50–500 ms, this strategy can save fabrication time as well as costs, which is suitable for mass production.

In conclusion, we propose a laser fabrication strategy that combines the 2PP and SLM to manufacture HAR microstructures by one-step exposure. The morphology of the micropillars can be adjusted flexibly by controlling the exposure height. The micropillars are suitable for the AFM probe. The LDOF probe has a comparable imaging quality compared with commercial ones, but is more advantageous in terms of economy and flexibility. This method greatly improves the processing efficiency while ensuring the fabrication resolution which provides a powerful method for processing HAR microstructures.

Funding. National Key R&D Program of China (2018YFB1105400, 2017YFB1104303); National Natural Science Foundation of China (61475149, 51675503, 51875544, 61805230, 51805508, 51805509); Fundamental Research Funds for the Central Universities (WK 2090090012, WK2480000002, WK2090090021, WK6030000103, WK6030000131); China Postdoctoral Science Foundation (2019M662190); Youth Innovation Promotion Association of the Chinese Academy of Sciences (2017495).

Acknowledgment. We acknowledge the Experimental Center of Engineering and Material Sciences at USTC for the fabrication and measuring of samples. This Letter was partly carried out at the USTC Center for Micro and Nanoscale Research and Fabrication.

Disclosures. The authors declare no conflicts of interest.

REFERENCES

- G. Binnig and H. Rohrer, *IBM J. Res. Dev.* **44**, 279 (2000).
- G. Binnig, C. F. Quate, and C. Gerber, *Phys. Rev. Lett.* **56**, 930 (1986).
- N. R. Wilson and J. V. Macpherson, *Nat. Nanotechnol.* **4**, 483 (2009).
- M. S. Bull, R. M. A. Sullan, H. Li, and T. T. Perkins, *ACS Nano* **8**, 4984 (2014).
- J. S. Lee, J. Song, S. O. Kim, S. Kim, W. Lee, J. A. Jackman, D. Kim, N. J. Cho, and J. Lee, *Nat. Commun.* **7**, 11566 (2016).
- J. M. Kim and H. Muramatsu, *Nano Lett.* **5**, 309 (2005).
- H.-B. Sun and S. Kawata, *NMR 3D Analysis Photopolymerization* (2006), Vol. **170**, pp. 169–273.
- L. Yang, A. El-Tamer, U. Hinze, J. Li, Y. Hu, W. Huang, J. Chu, and B. N. Chichkov, *Appl. Phys. Lett.* **105** 041110 (2014).
- G. Göring, P.-I. Dietrich, M. Blaicher, S. Sharma, J. G. Korvink, T. Schimmel, C. Koos, and H. Hölscher, *Appl. Phys. Lett.* **109** 063101 (2016).
- N. Alsharif, A. Burkatovsky, C. Lissandrello, K. M. Jones, A. E. White, and K. A. Brown, *Small* **14**, 1800162 (2018).
- K. Obata, J. Koch, U. Hinze, and B. N. Chichkov, *Opt. Express* **18**, 17193 (2010).
- N. Davidson, A. A. Friesem, and E. Hasman, *Opt. Lett.* **16**, 523 (1991).
- S. Ahlawat, R. S. Verma, R. Dasgupta, and P. K. Gupta, *Appl. Opt.* **50**, 1933 (2011).
- Z. Yao, L. Jiang, X. Li, A. Wang, Z. Wang, M. Li, and Y. Lu, *Opt. Express* **26**, 21960 (2018).
- C. Shen, Q. Hong, Q. Zhu, C. Zu, and S. Wei, *Opt. Laser Technol.* **120** 105682 (2019).

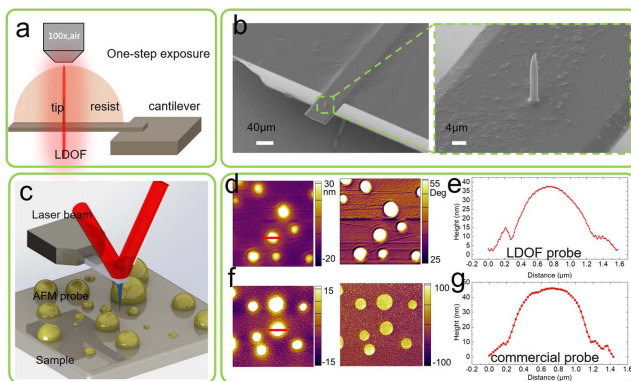


Fig. 4. LDOF probe and imaging test results. (a) Schematic diagram of fabricating the AFM tip by single exposure. (b) SEM images of AFM probe. (c) Diagram of AFM test. (d) Topography distribution and phase distribution results, respectively, measured using the LDOF probe. (e) Height information of the cross section marked in (d) (red line). (f) Topography distribution and phase distribution results, respectively, measured using the commercial probe. (g) Height information of the cross section marked in (f) (red line).